sustainability

MDPI

Technical Note

Mesoscopic Failure Behavior of Strip Footing on Geosynthetic-Reinforced Granular Soil Foundations Using PIV Technology

Zhongmei Wang [1,2], Zhiqiang Lai [1,2,*], Lianjun Zhao [1,2,*], Kangwei Lai [3] and Li Pan [1,2]

[1] Yellow River Institute of Hydraulic Research, Yellow River Conservancy Commission, Zhengzhou 450003, China
[2] Key Laboratory of Lower Yellow River Channel and Estuary Regulation, Ministry of Water Resources, Zhengzhou 450003, China
[3] School of Materials Science and Engineering, University of New South Wales, Sydney, NSW 2052, Australia
* Correspondence: laizhiqiang@hky.yrcc.gov.cn (Z.L.); zhaolianjun@hky.yrcc.gov.cn (L.Z.)

Abstract: Two-dimensional model tests combined with PIV technology were conducted to study the failure behavior of strip footing on geosynthetic-reinforced granular soil foundations on a mesoscale. The results showed that geosynthetic reinforcements improve the bearing capacity of granular soil foundations; however, the effectiveness of the reinforcement was affected by the position, length, and number of geosynthetics. The mesoscale factor affecting the reinforcement effectiveness was the size of the sliding wedge in the foundation, which was changed by the embedded geosynthetics. As the depth, length, number, and vertical spacing of the reinforcements varied, three possible failure modes occurred in the reinforced foundations: failure above the top reinforcement layer, failure between reinforcement layers, and failure similar to footings on the unreinforced foundation.

Keywords: sustainability; geosynthetics; reinforced granular soil foundation; meso-failure behavior; PIV technology

Citation: Wang, Z.; Lai, Z.; Zhao, L.; Lai, K.; Pan, L. Mesoscopic Failure Behavior of Strip Footing on Geosynthetic-Reinforced Granular Soil Foundations Using PIV Technology. *Sustainability* **2022**, *14*, 16583. https://doi.org/10.3390/su142416583

Academic Editor: Gianluca Mazzucco

Received: 16 November 2022
Accepted: 9 December 2022
Published: 11 December 2022

1. Introduction

Geosynthetics make infrastructure more sustainable. They extend the service life of the foundation of the roads, reduce the use of aggregates and minimize land disturbance [1–4]. Therefore, geosynthetics have been widely used in retaining walls [5–7], foundations [8,9] and slopes [10,11].

As a result of the large amount of experimental data accumulated around the world [12–15] and available computational capacity [16–18], the ultimate bearing capacity and the corresponding macroscopic failure modes of reinforced foundations have been investigated and verified with sufficient credibility using continuum mechanics. However, investigations on the responses of foundation systems, particularly the mesoscopic response of the underlying soil, have been relatively sparse and may be of great importance in deepening our understanding of macroscopic behavior.

Particle image velocimetry (PIV) has improved with the development of computers and signal processors. This technique can correlate two consecutive images and obtain their relative displacement. Therefore, it has been used to obtain the mesoscopic movement of soil particles in backfills around piles and slopes and behind walls [19–22]. In this study, a series of 2D model tests combined with PIV technology were conducted on granular soil foundations reinforced by geosynthetics of different lengths, top layer spacing, number of layers, and vertical spacing to investigate the mesoscopic responses of reinforced foundations. The responses included (i) the movement of underlying soil particles in a foundation, (ii) the mesoscopic failure mode of a reinforced soil foundation, and (iii) the effect of the position, length, and number of geosynthetics on the failure mode.

2. Experimental Investigation

2.1. Test Setup

Figure 1 shows a schematic diagram and photo of the 2D model tests performed in a containing box, measuring 120 × 10 × 100 cm (length × width × height), formed by three 1 cm thick iron walls, which were rigid enough without deformation. An assembly of 10 cm long aluminum rods was arranged to simulate the underlying soil particles of a foundation. As the aluminum rod assembly can stand on its own, and to avoid friction on the front and back, there is not a baffle at the front and the back of the containing box. The aluminum rods used have two diameters: 3 and 6 mm. The ratio of the mass of 3 mm rods to that of 6 mm rods is 3:2. The aluminum rod mass has a void ratio of 0.24 and a dry unit weight γ of 21.4 kN/m^3 [23]. The internal friction angle φ of the aluminum rod mass obtained from biaxial shear tests is 21.6°. The advantages of modeling soil particles using aluminum rods include that (i) the specific gravity G_s of aluminum (2.69) is close to that of native soils [12], (ii) there is no need to confine the front and back faces of the aluminum rods, and (iii) it is easy to capture the movement of the rods using PIV technology [21,24]. Geosynthetics made of polyethylene, with a weight of 87 g/m^2, were embedded horizontally within the aluminum rod foundation. Table 1 provides a summary of the geosynthetic properties with wide-width tensile testing.

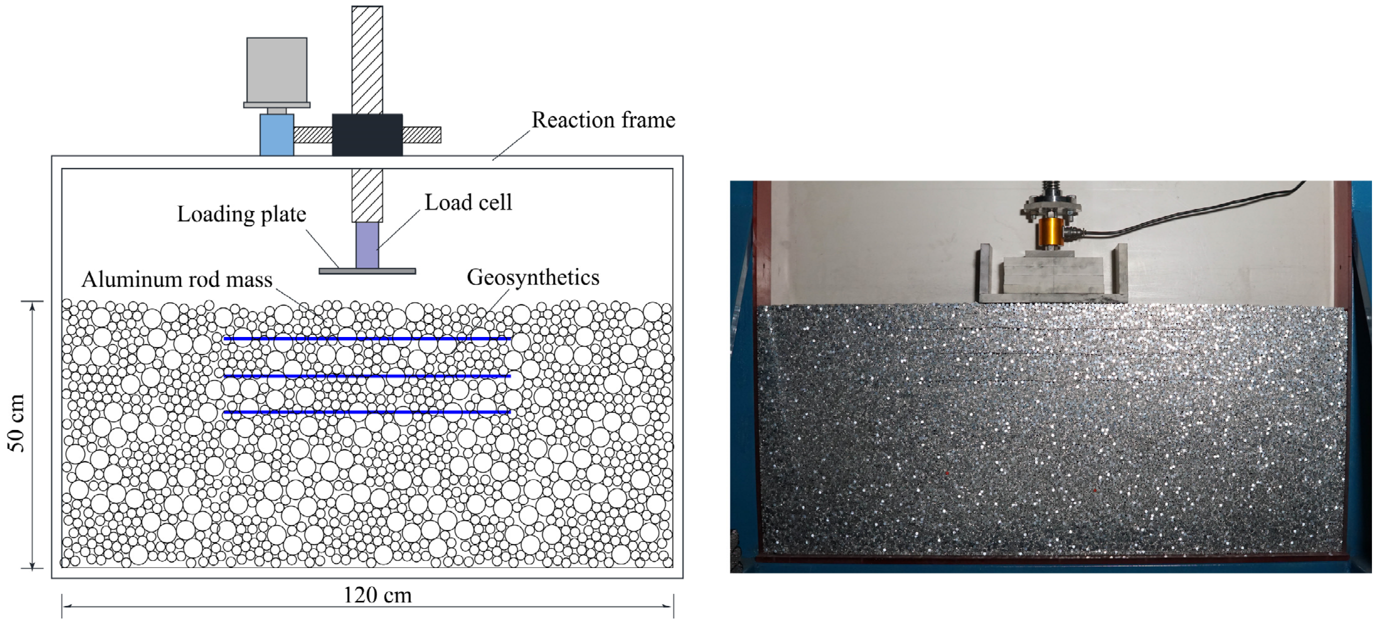

Figure 1. Schematic diagram and photo of 2D model test setup.

Table 1. Properties of geosynthetics.

Property	Value
Ultimate tensile strength (kN/m)	≥11.2
Tensile strength @2% strain (kN/m)	≥3.1
Tensile strength @5% strain (kN/m)	≥6.2
Peak strain (%)	≤6.3

An aluminum plate with a width B of 30 cm was placed on the surface of the rod to simulate the bearing capacity of a strip foundation. A vertical load was applied on a load plate which was placed in the middle of the rod surface, and the rate of the applied load was 6 mm/min. The applied load was increased until the vertical displacement reached 60 mm. A load cell was installed in the loading system to measure the load magnitude. A camera was positioned at front of the model box to photograph the foundation at a frequency of 4 s. The photographs were post-processed using PIV technology to derive the movement of the aluminum rods and the mesoscopic failure model of the foundation. In the 2D model tests, if the aluminum rods were the same size, it would be difficult to precisely capture the trajectories between them. Therefore, aluminum rods with diameters of 3 and 6 mm were chosen for the tests.

2.2. Test Scheme

For a given geosynthetic and soil type, the length of reinforcement *l*, top layer spacing *u*, number of layers *N*, and vertical spacing between geosynthetic reinforcements *h* (see Figure 2) influence the foundation-bearing capacity. To investigate the factors influencing the mesoscopic failure behavior of the reinforced foundations, four series of model tests were carried out in this study, and the purpose of each group and the corresponding conditions are summarized in Table 2. Having noted that the loading plate may contact the geosynthetics during the loading process if the buried depth of the first layer of geosynthetics is small, the value of 5 cm was chosen (i.e., 0.17 *B*) as the buried depth of the first layer of the geosynthetic in this study. Abu-Farsakh et al. [25] and Gill et al. [26] performed tests on geogrid reinforced foundations and suggested that the effective reinforcement depth was 1.25~2.5 *B*. Therefore, to study the effect of the burial depth of the first geogrid layer on the reinforced foundation-bearing capacity, the burial depth set in most documents was less than 1.25 *B*, and 0.05~1.0 *B* was always used [17,27–29]. In our studies, the burial depth of the first geogrid layer set was also in the range of 0.05~1.0 *B*.

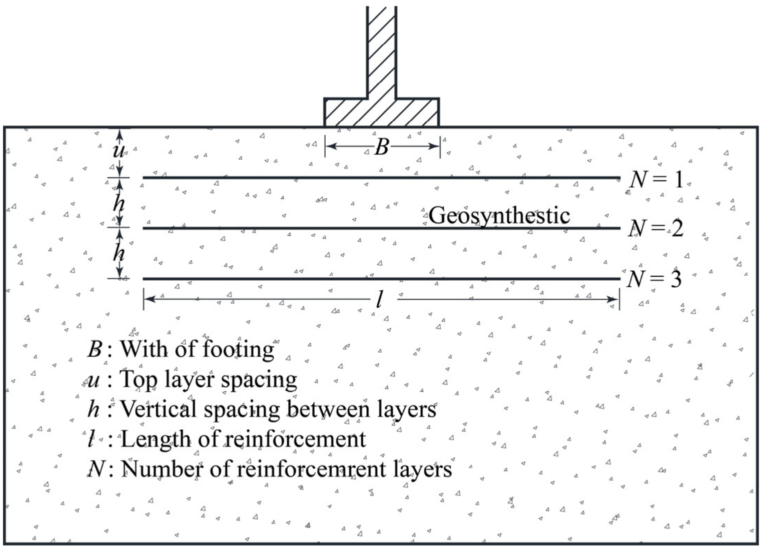

Figure 2. Geosynthetic-reinforced soil foundation parameters.

Table 2. Test group purposes and conditions.

Title 1	Title 2	Title 3
T0	Basic case for particle movement	Unreinforced
TN	Influence of layer number	Reinforced: u = 5 cm, h = 5 cm, l = 60 cm, N = 1, 2, and 3
Tl	Influence of length	Reinforced: u = 5 cm, h = 5 cm, l = 40, 60, and 80 cm, N = 1
Tu	Influence of top layer spacing	Reinforced: u = 5, 10, and 15 cm, h = 5 cm, l = 40 cm, N = 1
Th	Influence of vertical spacing	Reinforced; u = 5 cm, h = 5, 7.5, and 10 cm, l = 40 cm, N = 3

3. Test Results

3.1. Unreinforced Foundation

Figure 3 shows a plot of the applied load versus the settlement ratio (s/B) obtained from the tests on the unreinforced foundation. The load–settlement curves obtained from two separate tests were nearly identical, indicating the repeatability of the test system. The point at which the load–settlement relationship changed its inclination was defined as the bearing capacity of the foundation. The ultimate bearing-capacity value for strip footing, according to Terzaghi, was calculated as q_u = 25.9 kPa, using the formula $q_u = 0.5\gamma BN_\gamma$ [30]. The ultimate bearing-capacity value obtained from the test results (Figure 3) was close to the calculated value, indicating that the tests on the unreinforced foundation yielded true results. The cumulative displacement distributions of the soil particles without geosynthetics under an applied load of 25.9 kPa are plotted in Figure 4. A general shear failure mode that occurred in the soil specimen was similar to that of the DEM modeling results reported by Fu et al. [31]. This verified the reliability of the test system.

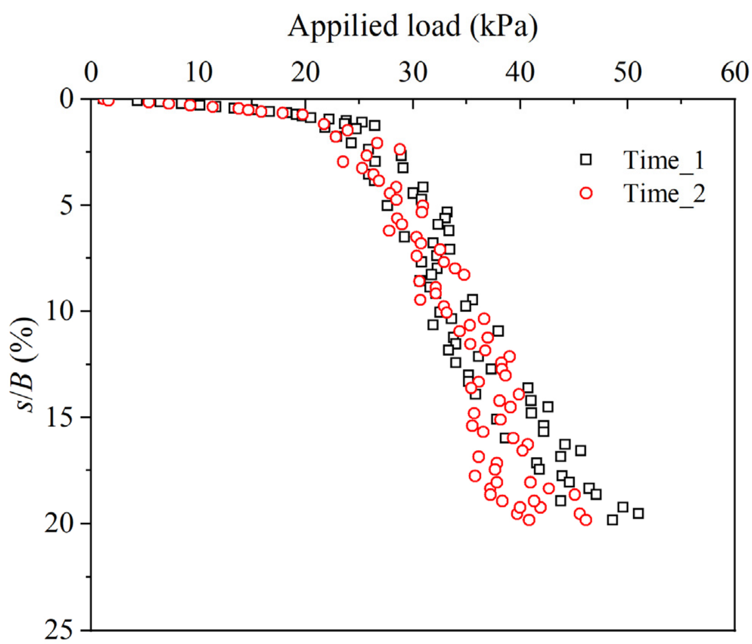

Figure 3. Vertical pressure versus settlement of the unreinforced foundation.

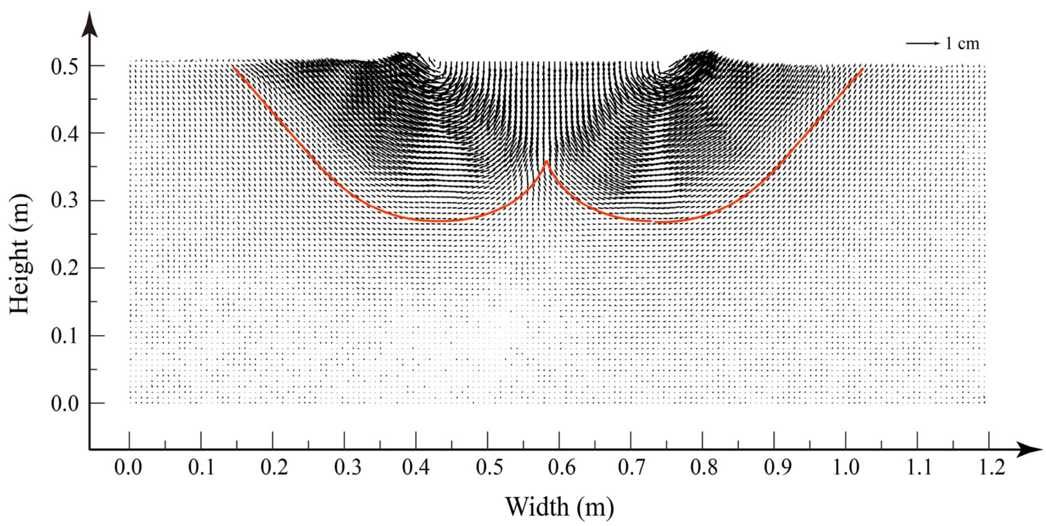

Figure 4. Cumulative movement of underlying particles in unreinforced foundation.

3.2. Influence of Layer Number

Generally, the bearing capacity of a foundation is enhanced by geosynthetics and increases with the number of reinforcement layers. Similar results were also obtained in this study (Figure 5). The ultimate bearing load of the reinforced foundation increased from 32.3 to 35.6 kPa as the layer number N increased from 1 to 2 and until 60.9 kPa, when N = 3. To analyze this result, the cumulative displacement distributions of soil particles in the reinforced foundations with different geosynthetic-layer numbers were investigated as the load approached the ultimate bearing load, as shown in Figure 6. The movement law of the aluminum rods in the reinforced foundation was the same as that in the unreinforced foundation; however, the displacement increased. To compare the displacement differences of the reinforced and unreinforced foundations, red lines were drawn where the displacement of the aluminum rods was equal to 1 mm, which is regarded as the failure surface of the foundation. Because of the pressure transfer behavior from the soil to the geogrids, the sliding wedges in the reinforced cases (N = 1, 2, and 3) were significantly larger than those in the case of N = 0 (see Figures 4 and 6). This resulted in an ultimate reinforced foundation-bearing load significantly larger than that of the unreinforced foundation. In other words, geosynthetics increased the size of the sliding wedge, and more force was required to push the wedge. Because the size of the sliding wedge in the N = 2 reinforced case was slightly greater, its ultimate bearing pressure was slightly greater. In the N = 3 reinforced case, the size of the sliding wedge was far greater than that of the N = 1 reinforced case, and the ultimate bearing pressure was far greater. It can be concluded that the micro mechanism of the increasing bearing capacity of the reinforced foundation caused by the increased number of geosynthetics is the increase in the size of the sliding wedge in the foundation.

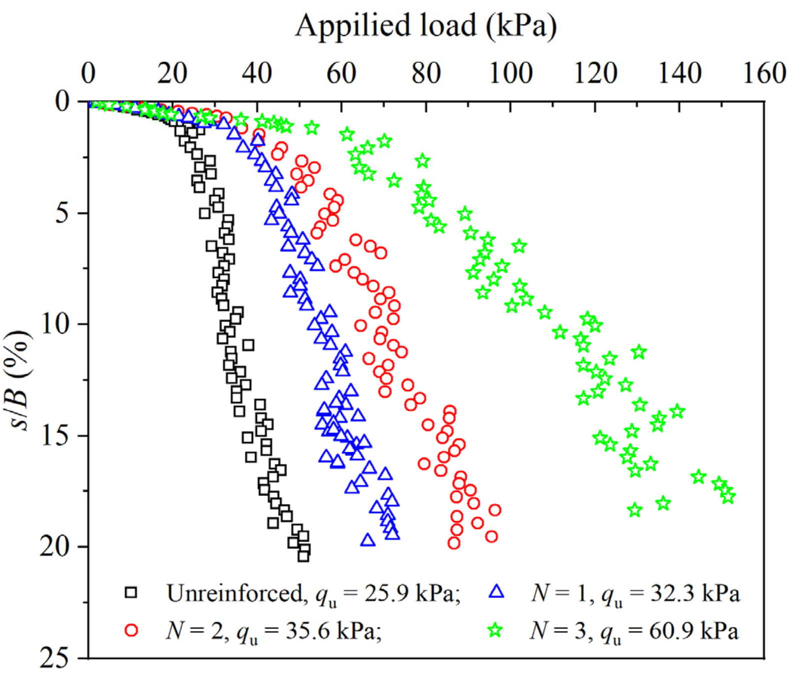

Figure 5. Load–settlement curves of reinforced foundations with different numbers of geosynthetic layers.

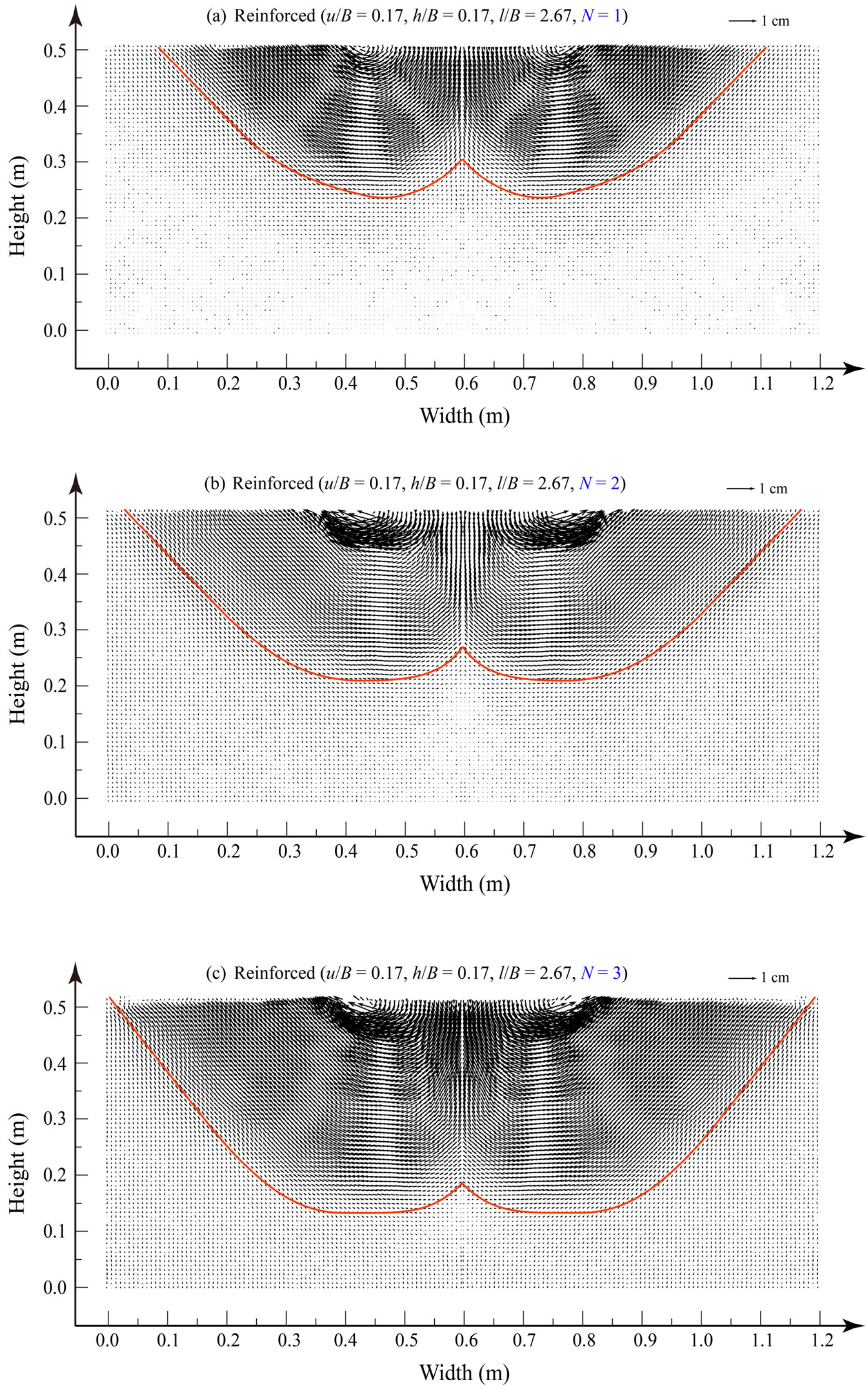

Figure 6. Effect of number of layers on failure models of reinforced foundations.

3.3. Influence of Length

Shahin et al. [17] studied the effect of reinforcement length l on the bearing capacity of reinforced foundations. They stated that a significant increase in the bearing capacity could be achieved if the geosynthetics were placed at an optimum length, and no significant change in the bearing capacity occurred when the reinforcement length was $l/B > 2$. In this study, the ultimate bearing load of the reinforced foundation increased from 28.3 to 33.1 kPa as l increased from 40 to 60 cm and increased to 36.3 kPa when l = 80 cm, as shown in Figure 7. Owing to model size limitations, tests on reinforced foundations with longer geosynthetics were not carried out.

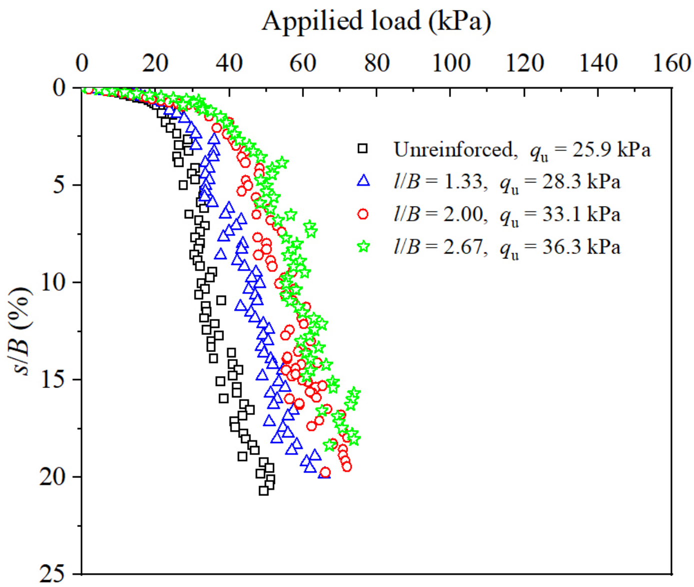

Figure 7. Effect of length *l* on load–settlement curves of reinforced foundations.

Figure 8 shows the sliding wedge of the foundation reinforced with geosynthetics of different lengths. With an increase in the length of the geosynthetics, the width of the sliding wedge increased, but the depth remained substantially unchanged. This is because the increase in the length of geosynthetics can only transfer the force to a wider range, not to a deeper range. Still, the ultimate bearing load increases with the increase in the sliding width. Because the increment of sliding width as *l* increases from 40 cm to 60 cm is greater than that from 60 cm to 80 cm, the increment of ultimate bearing load decreases from 4.8 kPa to 3.2 kPa.

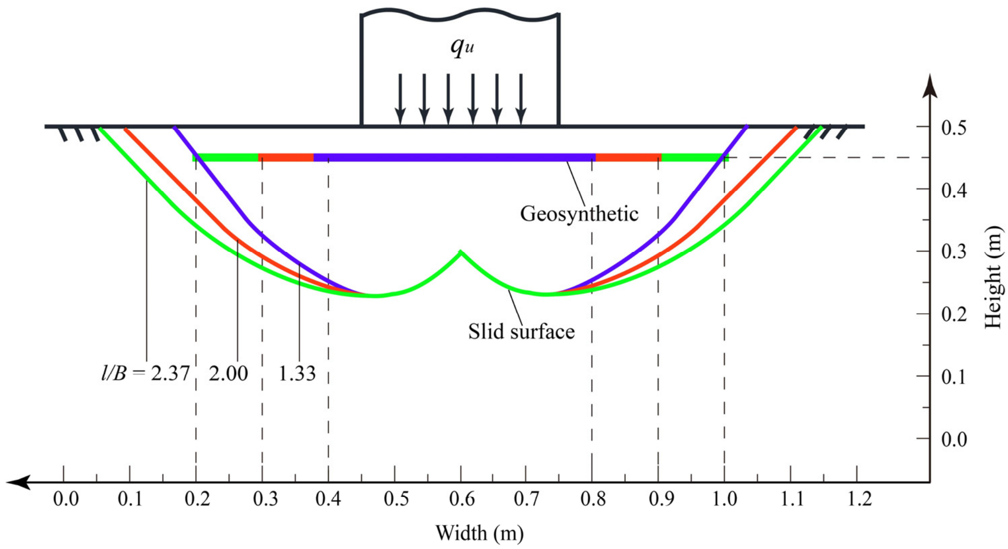

Figure 8. Effects of length *l* on failure models of reinforced foundation.

3.4. Influence of Top Layer Spacing

The sliding wedge and load–settlement curves for the model tests with one layer of reinforcement placed in different spaces are presented in Figures 9 and 10, respectively. When the top-layer spacing was relatively small (u/B = 0.17 and 0.33), a sliding wedge occurred in the unreinforced zone (purple and green lines). However, when the top layer spacing increased to 15 cm, the sliding surface slid directly along the contact surface between the geosynthetics and the soil, and a sliding wedge occurred in the reinforced zone (red lines). Because the size of the sliding wedge increased, the ultimate bearing load increased from 33.1 to 37.9 kPa as u/B increased from 0.17 to 0.33. Whereas the ultimate bearing load decreased to 20.3 kPa (even less than that of the unreinforced foundation) when u/B increased to 0.50 as the result of the decrease in the size of the sliding wedge. This finding was similar to that reported by Shin et al. [32] It has been noted that the friction at the soil–reinforcement interface in 3D model tests may be larger than that in 2D model tests; thus, the ultimate bearing load in the 3D model tests may increase even if the size of the sliding wedge decreases.

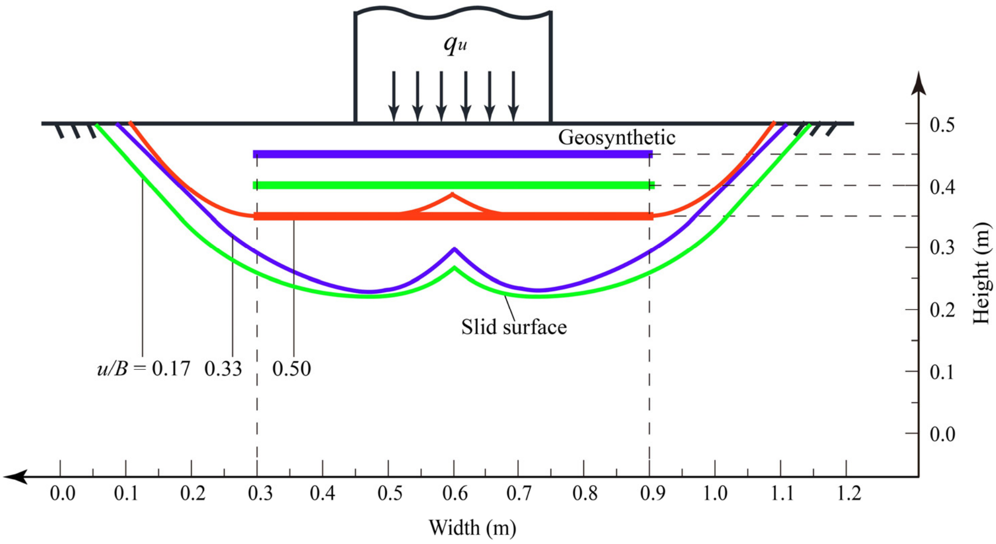

Figure 9. Effect of top layer spacing u on failure models of reinforced foundations.

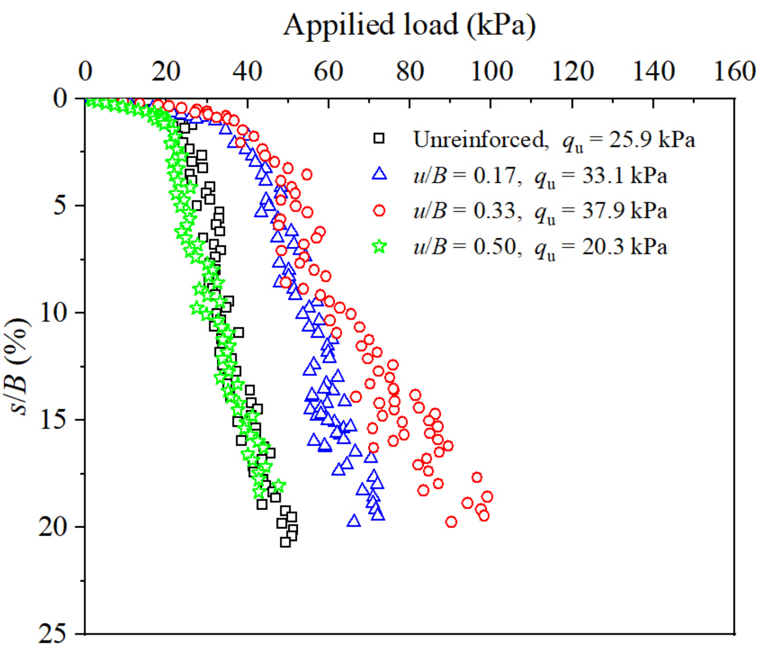

Figure 10. Effect of top layer spacing u on load–settlement curves of reinforced foundations.

3.5. Influence of Vertical Spacing

Figures 11 and 12 show the sliding wedge and load–settlement curves for the model tests with three layers of reinforcement placed at different vertical spacings. When the vertical spacing was relatively small (h/B = 0.17), a sliding wedge occurred in the unreinforced zone (purple line); however, the sliding wedge also occurred in the reinforced zone with h/B = 0.25 and 0.33 because the sliding surface slid directly along the contact surface between geosynthetic and soil. Because the size of the sliding wedge decreased as h/B increased from 0.17 to 0.25, the ultimate bearing load decreased from 60.9 to 32.4 kPa, whereas it increased from 32.4 to 38.1 kPa as h/B increased from 0.25 to 0.33.

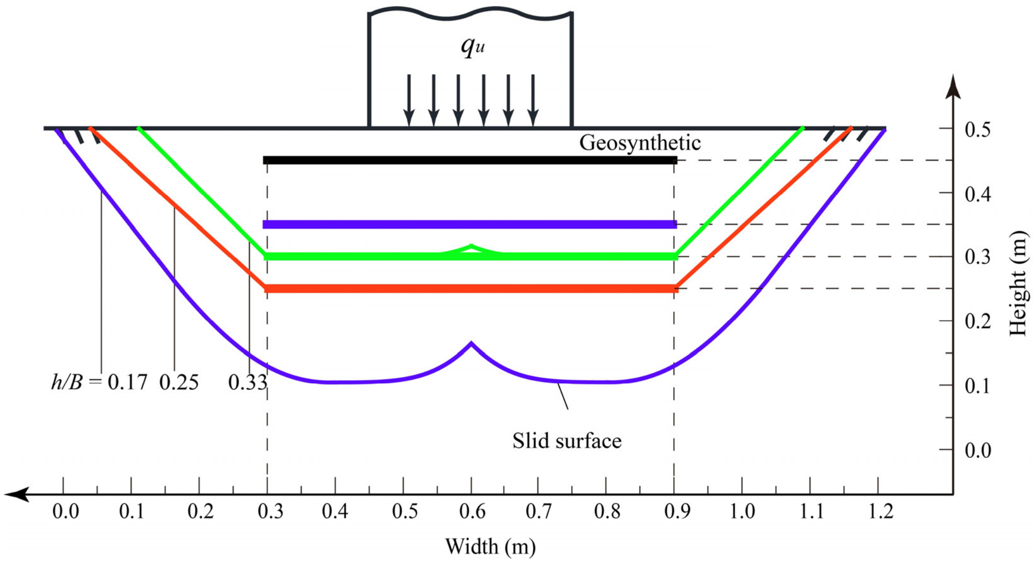

Figure 11. Effect of vertical spacing h on failure models of reinforced foundations.

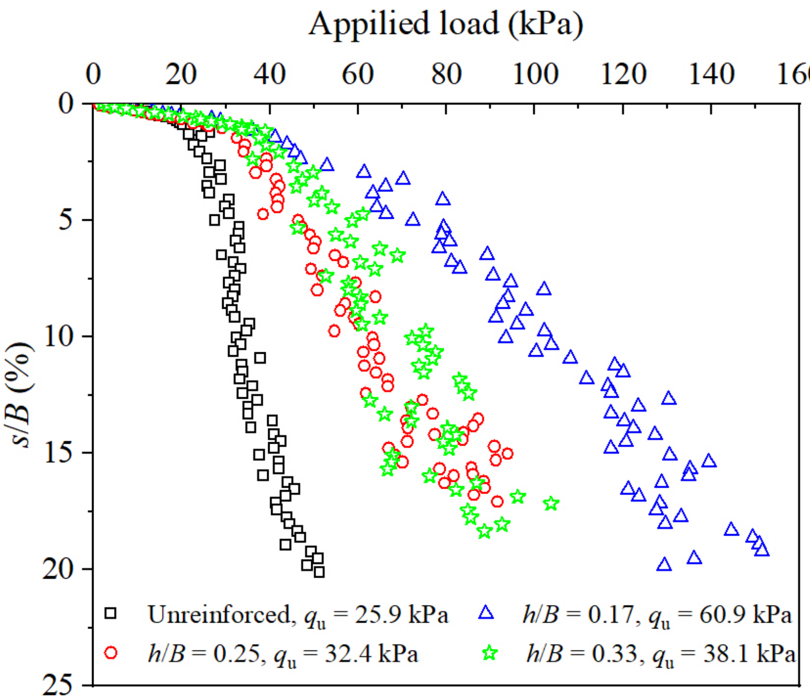

Figure 12. Effect of vertical spacing h on load–settlement curves of reinforced foundations.

3.6. Summary of Failure Model of Geosythetic-Reinforced Foundations

Based on the above 2D model test results, three possible failure modes are summarized for reinforced soil foundations as illustrated in Figure 13: failure above the top reinforcement layer, failure between reinforcement layers, and failure similar to footings on the unreinforced foundation. The first two failure modes should be avoided in engineering practice to fully exploit the reinforcement effect of geosynthetics. Abu-Farsakh et al. [33] conducted experimental studies and claimed that the first two failure modes can be avoided when the top layer spacing and vertical spacing are less than 0.5 *B*. Because 2D model tests were carried out in this study, the value of 0.5 *B* was not applicable here.

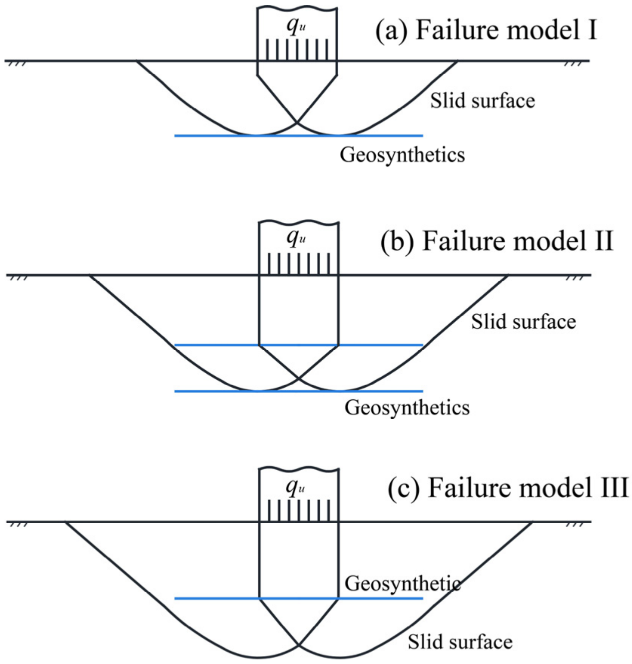

Figure 13. Failure models of reinforced foundation.

4. Conclusions

A series of 2D model tests were conducted to investigate the movement of soil particles, the failure models, and the bearing capacity of strip footing on unreinforced and reinforced foundations. Two-dimensional model tests on unreinforced foundations were conducted, and good agreement was observed between the test measurements and the Terzaghi bearing capacity theory for strip footing on unreinforced sand foundations. Tests on reinforced foundations were performed using different reinforcement depths, lengths, numbers, and vertical spacings. The conclusions are as follows:

(i) The reinforced micro mechanism of the embedded geosynthetics in improving the bearing capacity of the foundation is that the size of the sliding wedge in the foundation was changed.
(ii) When the buried depth and number of geosynthetics are within a certain range, they increase the depth of the sliding wedge in the foundation, whereas the length of the geosynthetics broadens the width of the sliding wedge.
(iii) Three possible failure modes may occur in reinforced foundations: failure above the top reinforcement layer, failure between reinforcement layers, and failure similar to footings on the unreinforced foundation.

Author Contributions: Z.W.: conceptualization, formal analysis, investigation, funding acquisition, validation, and writing of the original draft. Z.L.: methodology, investigation, project administration, writing—review and editing. L.Z.: supervision and methodology. K.L.: writing—review and editing, and formal analysis. L.P.: writing—review and editing. All authors have read and agreed to the published version of the manuscript.

Funding: This research was funded by the Key Commonwealth Project of Henan Province (Grant No. 201300311600), the National Natural Science Foundation of China (Grant No. 51909102), the Promotion and Transformation Fund of the Yellow River Institute of Hydraulic Research (Grant No. HKY-YF-2022-03) and the Central Public-interest Scientific Institution Basic Research Fund (Grant No. HKY-JBYW-2021-01).

Institutional Review Board Statement: Not applicable.

Informed Consent Statement: Not applicable.

Data Availability Statement: The data used to support the findings of this study are included within the article.

Acknowledgments: We would like to acknowledge the reviewers and editors for their valuable comments and suggestions.

Conflicts of Interest: The authors declare no conflict of interest.

Nomenclature

l	length of reinforcement (m)
u	top layer spacing (m)
N	number of layers
h	vertical spacing between reinforcements (m)
q_u	ultimate bearing capacity value for strip footing (kPa)
B	width of the aluminum plate
s	settlement of the aluminum plate

References

1. Palmeira, E.M.; Araújo, G.L.S.; Santos, E.C.G. Sustainable Solutions with Geosynthetics and Alternative Construction Materials—A Review. *Sustainability* **2021**, *13*, 12756. [CrossRef]
2. Cardile, G.; Pisano, M.; Recalcati, P.; Moraci, N. A new apparatus for the study of pullout behaviour of soil-geosynthetic interfaces under sustained load over time. *Geotext. Geomembr.* **2021**, *49*, 1519–1528. [CrossRef]
3. Shen, C.; Fan, K.; Liu, S.; Wang, L.; Lai, Z.; Yuan, W. A simple unified stress-strain model for geotextile-wrapped soils. *Geotext. Geomembr.* **2021**, *49*, 697–706. [CrossRef]
4. Zhu, Y.; Zhang, F.; Jia, S. Embodied energy and carbon emissions analysis of geosynthetic reinforced soil structures. *J. Clean. Prod.* **2022**, *370*, 133510. [CrossRef]
5. Liu, S.; Fan, K.; Xu, S. Field study of a retaining wall constructed with clay-filled soilbags. *Geotext. Geomembr.* **2019**, *47*, 87–94. [CrossRef]
6. Fan, K.; Liu, S.; Cheng, Y.P.; Wang, Y. Sliding stability analysis of a retaining wall constructed by soilbags. *Géotechnique Lett.* **2019**, *9*, 211–217. [CrossRef]
7. Wang, L.; Liu, S.; Liao, J.; Fan, K. Field load tests and modelling of soft foundation reinforced by soilbags. *Geosynth. Int.* **2019**, *26*, 580–591. [CrossRef]
8. Raja, M.N.A.; Shukla, S.K. Experimental study on repeatedly loaded foundation soil strengthened by wraparound geosynthetic reinforcement technique. *J. Rock Mech. Geotech.* **2021**, *13*, 899–911. [CrossRef]
9. Liu, S.; Liao, J.; Bong, T.T.; Fan, K. Repeated loading of soilbag-reinforced road subgrade. *Geosynth. Int.* **2021**, *28*, 113–124. [CrossRef]
10. Rimoldi, P.; Shamrock, J.; Kawalec, J.; Touze, N. Sustainable use of geosynthetics in dykes. *Sustainability* **2021**, *13*, 4445. [CrossRef]
11. Zhang, R.; Tang, P.; Lan, T.; Liu, Z.; Ling, S. Resilient and Sustainability Analysis of Flexible Supporting Structure of Expansive Soil Slope. *Sustainability* **2022**, *14*, 12813. [CrossRef]
12. Matsuoka, H.; Liu, S. New earth reinforcement method by soilbags ("donow"). *Soils Found.* **2003**, *43*, 173–188. [CrossRef] [PubMed]
13. Cicek, E.; Guler, E.; Yetimoglu, T. Effect of reinforcement length for different geosynthetic reinforcements on strip footing on sand soil. *Soils Found.* **2015**, *55*, 661–677. [CrossRef]
14. Ghazavi, M.; Lavasan, A.A. Interference effect of shallow foundations constructed on sand reinforced with geosynthetics. *Geotext. Geomembr.* **2008**, *26*, 404–415. [CrossRef]
15. Sharma, R.; Chen, Q.; Abu-Farsakh, M.; Yoon, S. Analytical modeling of geogrid reinforced soil foundation. *Geotext. Geomembr.* **2009**, *27*, 63–72. [CrossRef]
16. Abu-Farsakh, M.; Ardah, A.; Voyiadjis, G. 3D Finite element analysis of the geosynthetic reinforced soil-integrated bridge system (GRS-IBS) under different loading conditions. *Transp. Geotech.* **2018**, *15*, 70–83. [CrossRef]
17. Shahin, H.M.; Nakai, T.; Morikawa, Y.; Masuda, S.; Mio, S. Effective use of geosynthetics to increase bearing capacity of shallow foundations. *Can. Geotech. J.* **2017**, *54*, 1647–1658. [CrossRef]
18. Basudhar, P.K.; Dixit, P.M.; Gharpure, A.; Deb, K. Finite element analysis of geotextile-reinforced sand-bed subjected to strip loading. *Geotext. Geomembr.* **2008**, *26*, 91–99. [CrossRef]
19. Yuan, B.; Xu, K.; Wang, Y.; Chen, R.; Luo, Q. Investigation of deflection of a laterally loaded pile and soil deformation using the PIV technique. *Int. J. Geomech.* **2017**, *17*, 04016138. [CrossRef]
20. Baba, H.O.; Peth, S. Large scale soil box test to investigate soil deformation and creep movement on slopes by Particle Image Velocimetry (PIV). *Soil Till. Res.* **2012**, *125*, 38–43. [CrossRef]

21. Fan, K.; Yan, J.; Zou, W.; Han, Z.; Lai, Z. Active earth pressure on non-yielding retaining walls with geofoam blocks and granular backfills. *Transp. Geotech.* **2022**, *33*, 100712. [CrossRef]
22. Yuan, B.; Sun, M.; Wang, Y.; Zhai, L.; Luo, Q.; Zhang, X. Full 3D displacement measuring system for 3D displacement field of soil around a laterally loaded pile in transparent soil. *Int. J. Geomech.* **2019**, *19*, 04019028. [CrossRef]
23. Shen, C.; Liu, S.; Xu, S.; Wang, L. Rapid estimation of maximum and minimum void ratios of granular soils. *Acta Geotech.* **2019**, *14*, 991–1001. [CrossRef]
24. Xu, C.; Zhang, X.; Han, J.; Yang, Y. Two-dimensional soil-arching behavior under static and cyclic loading. *Int. J. Geomech.* **2019**, *19*, 04019091. [CrossRef]
25. Abu-Farsakh, M.; Chen, Q.; Sharma, R. An experimental evaluation of the behavior of footings on geosynthetic-reinforced sand. *Soils Found.* **2013**, *53*, 335–348. [CrossRef]
26. Gill, K.S.; Choudhary, A.K.; Jha, J.N.; Shukla, S.K. Experimental and numerical studies of loaded strip footing resting on reinforced fly ash slope. *Geosynth. Int.* **2013**, *20*, 13–25. [CrossRef]
27. Wang, J.; Zhang, L.; Xue, J.; Tang, Y. Load-settlement response of shallow square footings on geogrid-reinforced sand under cyclic loading. *Geotext. Geomembr.* **2018**, *46*, 586–596. [CrossRef]
28. Bildik, S.; Laman, M. Effect of geogrid reinforcement on soil-structure–pipe interaction in terms of bearing capacity, settlement and stress distribution. *Geotext. Geomembr.* **2020**, *48*, 844–853. [CrossRef]
29. Gao, J.; Liu, L.; Zhang, Y.; Xie, X. Deformation mechanism and soil evolution analysis based on different types geogrid reinforced foundation. *Constr. Build. Mater.* **2022**, *331*, 127322. [CrossRef]
30. Terzaghi, K. Liner-plate tunnels on the Chicago (Il) subway. *Trans. Am. Soc. Civ. Eng.* **1943**, *108*, 970–1007. [CrossRef]
31. Fu, Z.; Chen, S.; Liu, S. Discrete element simulations of shallow plate-load tests. *Int. J. Geomech.* **2016**, *16*, 04015077. [CrossRef]
32. Shin, E.C.; Das, B.M.; Puri, V.K.; Yen, S.C.; Cook, E.E. Bearing capacity of strip foundation on geogrid-reinforced clay. *Geotech. Test. J.* **1993**, *16*, 534–541.
33. Abu-Farsakh, M.; Chen, Q.; Sharma, R.; Zhang, X. Large-scale model footing tests on geogrid-reinforced foundation and marginal embankment soils. *Geotech. Test. J.* **2008**, *31*, 413–423.